## Supporting Information for
## "Forcing dependence of atmospheric lapse rate changes dominates residual polar warming in solar radiation management scenarios."

### Matthew Henry[1] and Timothy M. Merlis[1]

[1]Department of Atmospheric and Oceanic Sciences, McGill University, Montreal, Quebec, Canada.

## Contents

### Text S1: Lapse rate forcing dependence in analytic radiative-advective model of high latitude atmosphere[1].

We use an analytic model of the high latitude atmosphere in radiative-advective equilibrium: heating from atmospheric energy transport convergence is balanced by radiative cooling.

The temperature in this model is controlled by three factors: surface forcing $F_S$, atmospheric forcing $F_A$ and longwave optical depth $\tau_0$. The model is always at equilibrium, thus the sum of surface forcing ($F_S$) and atmospheric forcing ($F_A$) is balanced by the outgoing longwave radiation (OLR). The atmospheric forcing ($F_A$) includes atmospheric solar absorption, but since most of the solar radiation is absorbed at the surface, an increase in the solar forcing is modelled as an increase in the surface forcing $F_S$.

We use this analytic model to understand why, for an atmosphere in radiative-advective equilibrium, the lapse rate change for an increase in longwave optical depth is more bottom-heavy than for an increase in surface forcing. The equations and results from Cronin & Jansen[1] are reproduced here as we use a simpler pure radiative version of this model in the main text.

The two-stream Schwartzchild equations for gray radiative transfer with no atmospheric window are:

$$\frac{\partial F_+}{\partial \tau} = F_+ - \sigma T^4$$

$$\frac{\partial F_-}{\partial \tau} = -F_- + \sigma T^4,$$

where $(\frac{\tau}{\tau_0}) = (\frac{p}{p_0})^2$ with $\tau$ the longwave optical depth, $\tau_0$ the total longwave optical depth, $p$ the pressure and $p_0$ the surface pressure, $F_+$ is the upward longwave radiative flux, $F_-$ is the downward longwave radiative flux, $F$ is the net longwave radiative flux ($F = F_+ - F_-$), $I$ is the intensity ($I = F_+ + F_-$) and $T$ is the temperature of the atmospheric column.

We can rewrite these equations as a function of net flux ($F$) and intensity ($I$) and rearrange:

Corresponding author: Matthew Henry, `matthew.henry@mail.mcgill.ca`

$$2\sigma T(\tau)^4 = I(\tau) - \frac{\partial F}{\partial \tau}(\tau) \tag{1}$$

$$I(\tau) = \int_0^\tau F(\tau')d\tau' \tag{2}$$

In this simplification of the analytic model of radiative-advective equilibrium, the vertical structure of temperature changes is mainly determined by radiative intensity changes (equation 1) as $\frac{\partial F}{\partial \tau}$ is vertically uniform given that the net flux decreases linearly with respect to optical depth. Radiative intensity (I) can be calculated as the integral of net radiative flux with respect to optical depth (equation 2). Using the boundary conditions for the net radiative flux (F), it is shown that radiative intensity has a more bottom-heavy change in the case of increasing longwave optical depth than it does from decreasing the surface forcing. Hence, the lapse rate change is forcing-dependent.

Figure S10 shows the net flux with respect to optical depth for the control case ("Control", black), the decreased surface forcing case ("Solar", yellow), and increased total longwave optical depth case ("$CO_2$", red). The net flux at $\tau = 0$ is the sum of the surface forcing (Fs) and the atmospheric forcing (Fa) (30 $W\,m^{-2}$ and 150 $W\,m^{-2}$ respectively in the "Control" experiment), and the net flux at $\tau = \tau_0$ is the surface forcing (30 $W\,m^{-2}$ in the "Control" experiment). The atmospheric heating is distributed linearly with respect to optical depth, hence the net flux increases linearly with optical depth in figure S10. While figure S10 is plotted with respect to optical depth, figure S9 is plotted with respect to pressure: the optical depth at the surface is always equal to the total optical depth (3 for the "Control" and "Solar" experiments and 3.2 for the "$CO_2$" experiment) and recall that $(\frac{\tau}{\tau_0}) = (\frac{p}{p_0})^2$. Figure S9c shows the change in radiative intensity for both cases. The radiative intensity can be calculated as the integral of the net flux with respect to optical depth ($\tau$) (equation 2). Given how the net flux changes, the change in intensity is more bottom-heavy in the $CO_2$ case than in the solar case.

In summary, the forcing dependence of the lapse rate response is caused by the boundary conditions of the net flux: $F_S$ at the surface and $F_S + F_A$ at the TOA. In the increased total longwave optical depth case, the boundary conditions stay the same, however the atmosphere deepens with respect to optical depth, which constrains the intensity to a constant value at the TOA and to increase monotonically with pressure. This leads to a bottom-heavy change in intensity and a very bottom-heavy change in temperature. In the surface forcing case, the two boundary conditions of the net flux change equally, which reduces the net flux everywhere. This, in turn, leads to a less bottom-heavy decrease in the intensity, which induces a less bottom-heavy temperature change. Similarly, if the atmospheric forcing were increased, the bottom boundary condition would not change but the top boundary condition would increase, leading to an almost vertically uniform intensity increase and hence temperature change[1].
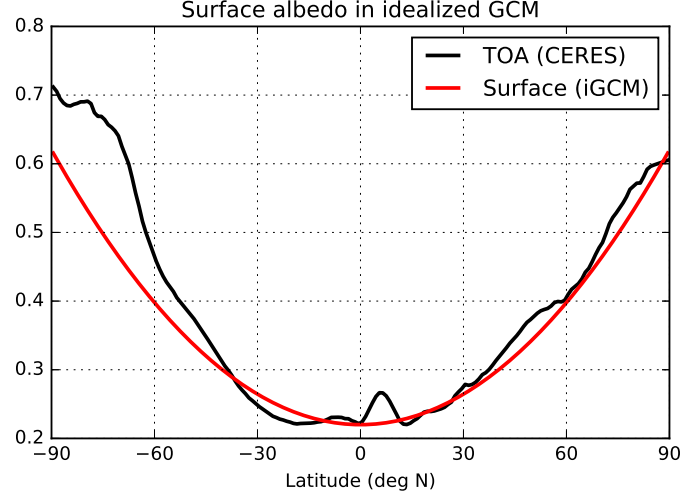
**Figure S1.** Surface albedo used in idealized GCM calculated using following formula: $0.22 + 0.4 * (lat/90)^2$ (red). Annual-mean zonally averaged climatology (07/2005 - 06/2015) of top-of-atmosphere albedo with data from Cloud and the Earth's Radiant Energy System (CERES) (black).
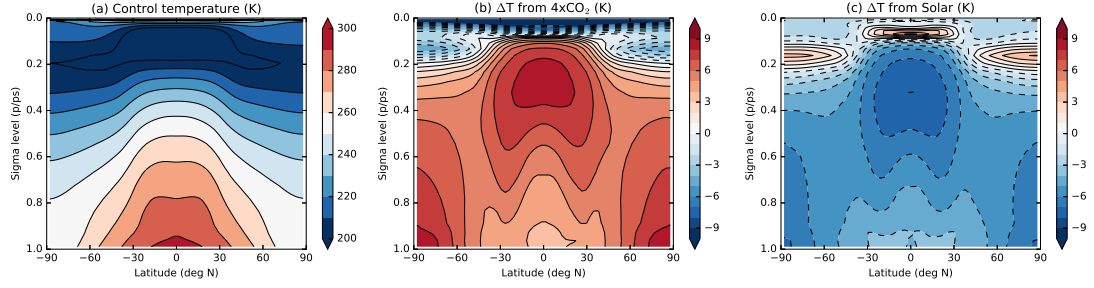


**Figure S2.** GFDL atmospheric GCM with comprehensive radiation, no clouds, aquaplanet surface boundary condition, and Earth-like TOA albedo (see figure S1) imposed at the surface to compensate for cloud cooling effect. Control temperature (a) and temperature change between control simulation and increased $CO_2$ simulation (b) and reduced solar constant simulation (c).
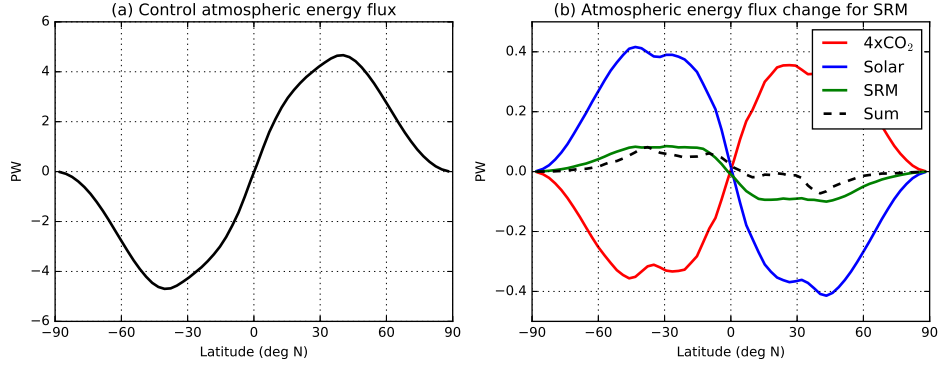
**Figure S3.** GFDL atmospheric GCM with comprehensive radiation, no clouds, aquaplanet surface boundary condition with TOA albedo imposed at the surface to compensate for cloud cooling effect. Control atmospheric energy transport (a) and change in atmospheric energy transport between control simulation and three other experiments ('4xCO$_2$', 'Solar', 'SRM') (b).
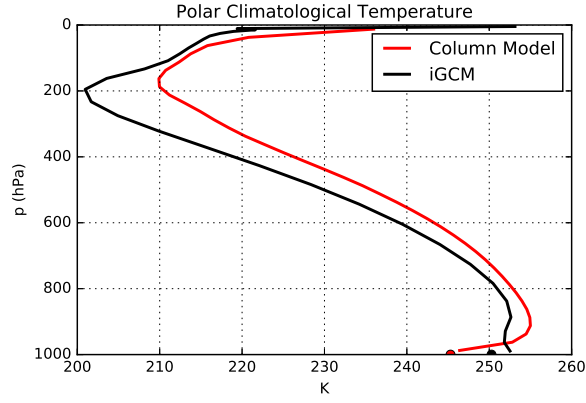


**Figure S4.** Control temperature poleward of 80 $^\circ$ North for single column model (red) and idealized GCM (black).
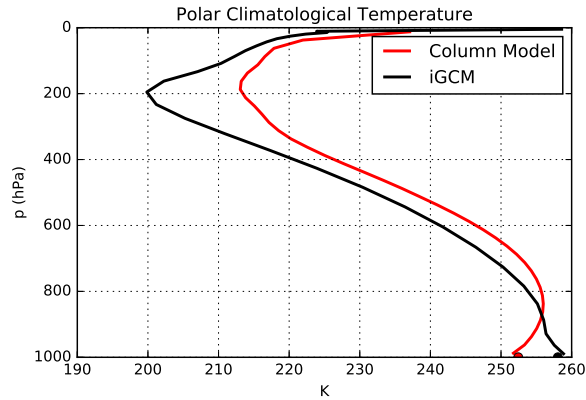


**Figure S5.** Control temperature poleward of 60$^\circ$ North for single column model (red) and idealized GCM (black). Same as figure S4 with 60$^\circ$ North latitudinal boundary.
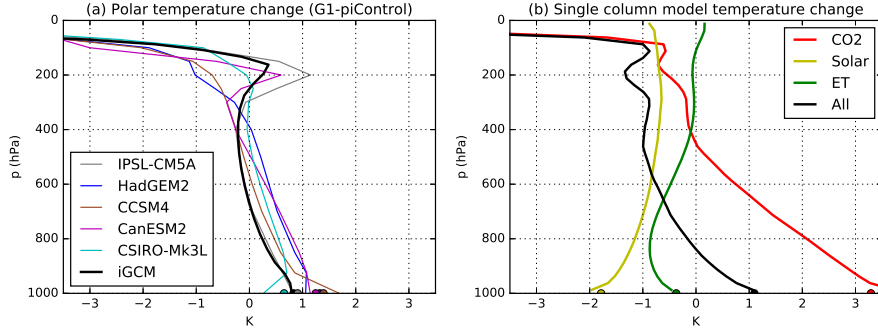
**Figure S6.** Same as figure 2 in main text with 60° North latitudinal boundary. (a) Temperature difference between solar geoengineered simulation (G1) and control simulation (piControl) in the Arctic (>60° North) for the idealized GCM (black) and comprehensive GCM simulations (colors, listed in legend). (b) Decomposition of polar temperature change using the single column model: increased $CO_2$ (red), reduced insolation (yellow), decreased energy transport (green), and all perturbations (black).
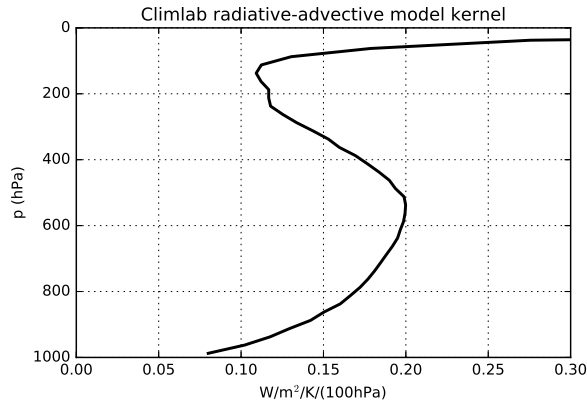


**Figure S7.** Climlab radiative-advective model temperature kernel. The temperature of the surface and each pressure level are independently increased by 1K, the temperature kernel is the resulting increase in OLR. The atmospheric kernel values are scaled such that their unit is $W\,m^{-2}\,K^{-1}\,(100hPa)^{-1}$. The surface kernel is 1.2 $W\,m^{-2}\,K^{-1}$ and the integrated atmospheric kernel is 1.7 $W\,m^{-2}\,K^{-1}$. This is consistent with the temperature kernel in high latitudes from comprehensive GCMs[2].
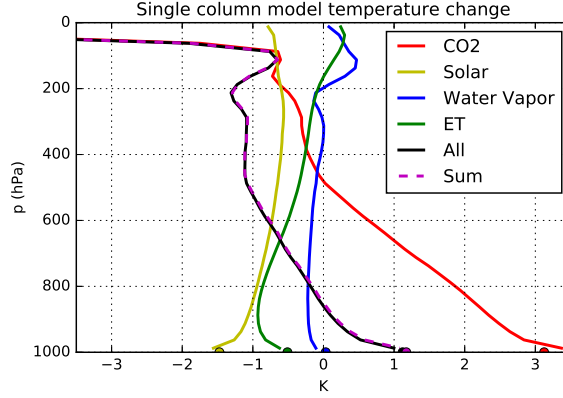
**Figure S8.** Same as figure 2b in the main text. Decomposition of polar temperature change using the single column model: increased $CO_2$ (red), reduced insolation (yellow), decreased energy transport (green), water vapor feedback (blue) and all perturbations (black). The sum of individual perturbations (dashed, magenta) matches the all perturbations temperature change.
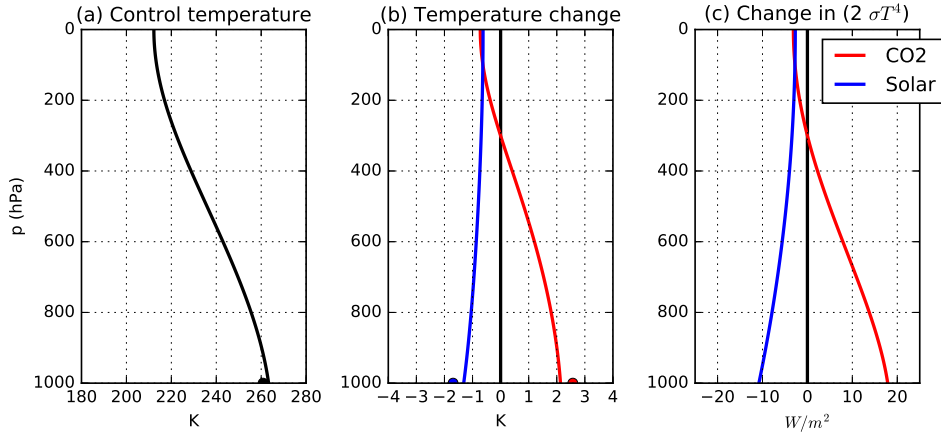


**Figure S9.** Analog of figure 3 in main text for an atmosphere in radiative-advective equilibrium. One control experiment ($\tau_0 = 3$, $F_S = 30$ W m$^{-2}$ and $F_A = 150$ W m$^{-2}$) and two perturbation experiments where the total longwave optical depth ("$CO_2$", $\tau_0 = 3.2$) is increased and the surface forcing ("Solar", $F_S = 27.3$ W m$^{-2}$) is reduced. (a) Temperature of control experiment, (b) change in temperature and (c) change in intensity ($2\sigma T^4$).
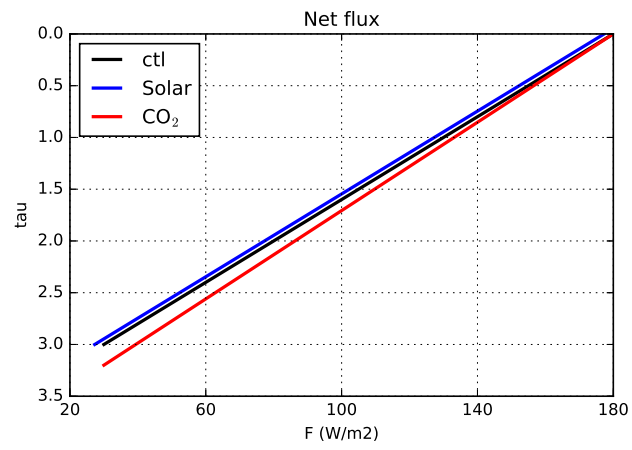
**Figure S10.** Change in net flux for radiative equilibrium experiments shown in figure S9.

| Run name | $CO_2$ conc (ppm) | Insolation ($\mathrm{W\,m^{-2}}$) | Specific humidity[a] | T tendencies[a] |
|---|---|---|---|---|
| Control | 300 | 175.2 | Control | Control |
| '4x$CO_2$' | 1200 | 175.2 | Control | Control |
| 'Solar' | 300 | 169 | Control | Control |
| 'ET' | 300 | 175.2 | Control | SRM |
| 'All' | 1200 | 169 | SRM | SRM |

**Table S1.** Parameter variations for climlab radiative-advective model simulations.

[a]These columns refer to the idealized GCM simulations from which we get the prescribed specific humidity and temperature tendency (advection and condensation) profiles.

# References

[1]  Cronin, T. W., & Jansen, M. F.   (2016).   Analytic radiative-advective equilibrium as a model for high-latitude climate.   *Geophysical Research Letters*, *43*(1), 449–457.

[2]  Soden, B. J., Held, I. M., Colman, R., Shell, K. M., Kiehl, J. T., & Shields, C. A.  (2008).  Quantifying climate feedbacks using radiative kernels.  *J. Climate*, *21*, 3504–3520.